# Quasi-Phase-Matched Supercontinuum Generation in Photonic Waveguides

Daniel D. Hickstein,[1,*] Grace C. Kerber,[1,2] David R. Carlson,[1] Lin Chang,[3] Daron Westly,[4] Kartik Srinivasan,[4] Abijith Kowligy,[1] John E. Bowers,[3] Scott A. Diddams,[1,5] and Scott B. Papp[1,5]

[1]*Time and Frequency Division, National Institute of Standards and Technology, Boulder, Colorado 80305, USA*
[2]*Gustavus Adolphus College, Saint Peter, Minnesota 56082, USA*
[3]*Department of Electrical and Computer Engineering, University of California, Santa Barbara, California 93106, USA*
[4]*Center for Nanoscale Science and Technology, NIST, Gaithersburg, Maryland 20899, USA*
[5]*Department of Physics, University of Colorado, Boulder, Colorado 80309, USA*

(Received 10 October 2017; published 1 February 2018)

Supercontinuum generation (SCG) in integrated photonic waveguides is a versatile source of broadband light, and the generated spectrum is largely determined by the phase-matching conditions. Here we show that quasi-phase-matching via periodic modulations of the waveguide structure provides a useful mechanism to control the evolution of ultrafast pulses during supercontinuum generation. We experimentally demonstrate a quasi-phase-matched supercontinuum to the $TE_{20}$ and $TE_{00}$ waveguide modes, which enhances the intensity of the SCG in specific spectral regions by as much as 20 dB. We utilize higher-order quasi-phase-matching (up to the 16th order) to enhance the intensity in numerous locations across the spectrum. Quasi-phase-matching adds a unique dimension to the design space for SCG waveguides, allowing the spectrum to be engineered for specific applications.

DOI: 10.1103/PhysRevLett.120.053903

Supercontinuum generation (SCG) is a $\chi^{(3)}$ nonlinear process where laser pulses of relatively narrow bandwidth can be converted into a continuum with large spectral span [1–3]. SCG has numerous applications, including self-referencing frequency combs [4–6], microscopy [7], spectroscopy [8], and tomography [9]. SCG is traditionally accomplished using bulk crystals or nonlinear fiber, but recently, photonic waveguides (on-chip waveguides produced using nanofabrication techniques) have proven themselves as a versatile platform for SCG, offering small size, high nonlinearity, and increased control over the generated spectrum [10–19]. The spectral shape and efficiency of SCG are determined by the input pulse parameters, the nonlinearity of the material, and the refractive index of the waveguide, which determines the phase-matching conditions.

Specifically, when phase matching between a soliton and quasicontinuous-wave light is achieved, strong enhancements of the intensity of the supercontinuum spectrum can occur in certain spectral regions. These spectral peaks are often referred to as a dispersive waves (DWs) [2,20–22], and they are often crucial for providing sufficient spectral brightness for many applications. The soliton-DW phase-matching condition is typically satisfied by selecting a material with a favorable refractive index profile and engineering the dimensions of the waveguide to provide DWs at the desired wavelengths [15,16]. However, there are limitations to the refractive index profile that can be achieved by adjusting only the waveguide cross section. Quasi-phase-matching (QPM) takes a different approach, utilizing periodic modulations of the material nonlinearity to achieve an end result similar to true phase matching [23–26]. QPM is routinely employed to achieve high conversion efficiency for nonlinear processes such as second-harmonic generation and difference-frequency generation, and QPM can also be used to satisfy the phase-matching conditions for DW generation [27–31].

Here we show that periodic modulations of the effective mode area can enable QPM of DW generation in photonic silicon nitride ($Si_3N_4$) waveguides, enhancing the intensity of the supercontinuum in specific spectral regions determined by the modulation period. Experimentally, we utilize a sinusoidal modulation of the waveguide width to enable first-order QPM to the $TE_{20}$ mode. Additionally, we demonstrate that periodic $SiO_2$ undercladding provides numerous orders of QPM to both the $TE_{20}$ and $TE_{00}$ modes. This quasi-phase-matched dispersive-wave (QPM-DW) scheme provides a fundamentally different approach to phase matching in SCG, allowing light to be generated outside the normal wavelength range, and providing separate control over the group-velocity dispersion (GVD) of the waveguide (which influences soliton propagation) and DW phase matching, capabilities that are desirable for many applications of SCG.

In the regime of anomalous GVD, the nonlinearity of the material can balance GVD and allow pulses to propagate while remaining temporally short. Such solitons can propagate indefinitely, unless perturbed [2,3]. However, in the presence of higher-order dispersion, some wavelengths of quasicontinuous-wave light may propagate at the same phase velocity as the soliton. Light at these wavelengths can "leak out" of the soliton in the form of DW radiation [2], which is also referred to as "resonant radiation" [20,21] or "optical Cherenkov radiation" [22].

 

In the SCG process, higher-order solitons undergo soliton fission and can convert significant amounts of energy into DW radiation [2]. The phase-matching condition for DW generation (in the absence of QPM) is simply [22]

$$n(\lambda_s) + (\lambda - \lambda_s)\frac{dn}{d\lambda}(\lambda_s) + \gamma p\lambda = n(\lambda), \tag{1}$$

where $\lambda$ is wavelength, $\lambda_s$ is the center wavelength of the soliton, $n$ is the effective index of the waveguide, $(dn/d\lambda)(\lambda_s)$ is the slope of the $n$-versus-$\lambda$ curve evaluated at $\lambda_s$, $\gamma$ is the effective nonlinearity of the waveguide, and $p$ is the peak power. The left side of Eq. (1) represents the effective index of the soliton while the right side represents the effective index of the DW. This equation has a simple graphical interpretation; because all wavelengths in the soliton travel with the same group velocity, the effective index of the soliton is simply a straight line [Fig. 1(c)]. Where this line crosses the refractive index curve for any waveguide mode [black lines in Fig. 1(c)] DW generation is phase matched.

Periodic modulations of the waveguide change the effective area of the mode, modulating both $\gamma$ and the GVD, enabling QPM-DW generation (see Supplemental Material [32], Sec. IV). The contribution of a modulation (with period $\Lambda$) to the wave vector phase mismatch will be $k_{QPM} = 2\pi q/\Lambda$, where $q$ is the QPM order and can be any positive or negative integer. Thus, the phase-matching condition for dispersive wave generation, in the presence of QPM is

$$\underbrace{n(\lambda_s) + (\lambda - \lambda_s)\frac{dn}{d\lambda}(\lambda_s) + \gamma p\lambda_s}_{\text{Soliton index}} = \underbrace{n(\lambda)}_{\text{DW index}} + \underbrace{\frac{2\pi q\lambda}{\Lambda}}_{\text{QPM}}. \tag{2}$$

This phase-matching condition has a similar graphical interpretation; an additional line is drawn for each QPM order, with curve crossings indicating QPM of DWs [Fig. 1(c)].

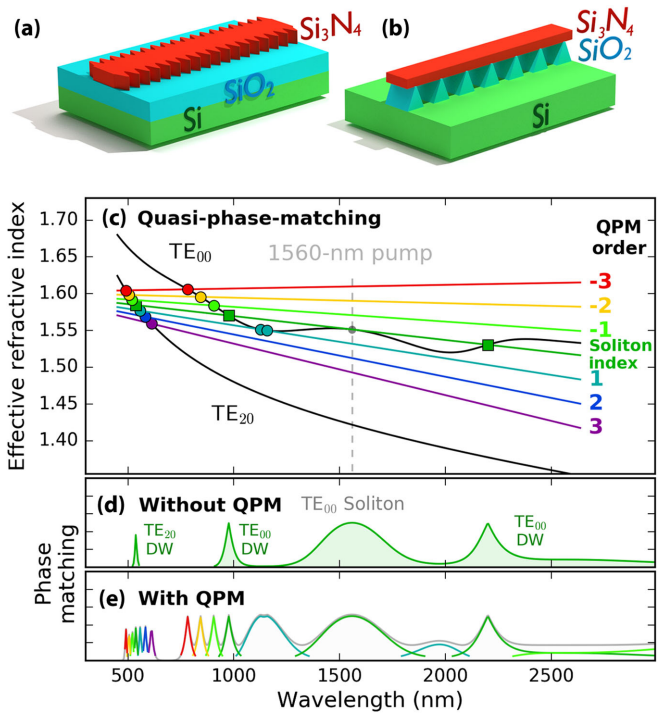


FIG. 1. (a), (b) Quasi-phase-matching of supercontinuum generation in on-chip photonic waveguides can be achieved via waveguide-width modulation (a) or cladding modulation (b). (c) When the effective index of the soliton in the $TE_{00}$ mode ("soliton index") intersects the effective index of a waveguide mode (black curves), phase matching to dispersive waves is achieved (green squares) and a spectrum with several peaks (d) is generated. The periodic modulation of the waveguide can enable numerous QPM orders, both positive and negative, which can allow QPM-DW generation to the fundamental mode and to higher-order modes (circles), producing a spectrum with many peaks (e). Note that the index curvature is exaggerated to better show phase matching.

In addition to satisfying the QPM condition [Eq. (2)], three additional requirements must be met for efficient DW generation. (i) The QPM order $q$ must be a strong Fourier component of the periodic modulation. (ii) There must be overlap between the spatial mode of the soliton and the mode of the DW. (iii) The DW must be located in a spectral region where the soliton has significant intensity, a requirement that applies regardless of the phase-matching method.

Experimentally, we explore two different approaches for QPM-DW generation in $Si_3N_4$ waveguides: width-modulated waveguides [33] and cladding-modulated waveguides. The width-modulated $Si_3N_4$ waveguides [Fig. 1(a)] are fully $SiO_2$ clad and have a thickness of 750 nm, a maximum width of 1500 nm, and an overall length of 15 mm. Over a 6-mm central region, the width is modulated sinusoidally from 1250 to 1500 nm. Multiple waveguides are fabricated on the same silicon chip, and each waveguide has a different width modulation period, which ranges from 5.5 to 6.5 μm. Each cladding-modulated waveguide [Fig. 1(b)] consists of a 700-nm-thick $Si_3N_4$ slab that is completely air clad, except for underlying $SiO_2$ support structures. The support structures are placed every 200 μm along the waveguide, and each one contacts the $Si_3N_4$ waveguide for approximately 20 μm. For the cladding-modulated waveguides, the modulation period is kept constant, but several waveguide widths are tested, ranging from 3000 to 4000 nm.

We generate supercontinuum by coupling ~80 fs pulses of 1560-nm light from a compact 100 MHz Er-fiber frequency comb [34]. The power is adjusted using a computer-controlled rotation mount containing a half-wave plate, which is placed before a polarizer. The polarization is set to horizontal (i.e., parallel to the Si-wafer surface and along the width dimension of the rectangular $Si_3N_4$ waveguide), which excites the lowest order quasitransverse-electric ($TE_{00}$) mode of the waveguide. We record the spectrum at many increments of the input power using an automated system [35] that interfaces with both the rotation mount and the optical spectrum analyzers. The waveguide modes (and

their effective indices) are calculated using a vector finite-difference mode solver [36,37], using published refractive indices for $Si_3N_4$ [38] and $SiO_2$ [39]. Further experimental details are found in the Supplemental Material [32].

For the width-modulated waveguides, a narrow peak appears in the spectrum in the 630-nm region [Fig. 2(a)], and the location of this peak changes with the width-modulation period [Fig. 2(c)]. By calculating the refractive index of the higher order modes of the waveguide, and including the QPM effect from the periodic width modulation [Fig. 2(b) and Eq. (2)], we find the QPM-DW generation to the $TE_{20}$ mode is a likely mechanism for the appearance of this peak [Fig. 2(c)]. The preference for QPM-DW generation to the $TE_{20}$ mode is a result of the modal overlap [3,40] (Fig. 3) between the $TE_{20}$ mode at the DW wavelength (~630 nm) and the $TE_{00}$ mode at the soliton wavelength (1560 nm). In general, modes that are symmetric in both the vertical and horizontal directions (such as the $TE_{20}$ mode) will have much higher overlap with the fundamental mode than antisymmetric modes (see Supplemental Material [32], Sec. III), and are, consequently, the most commonly used for model phase-matching schemes [41].

For the cladding-modulated waveguides, many QPM-DW peaks are seen in the supercontinuum spectrum [Fig 4(a)]. In some cases, the enhancement in the spectral intensity is as high as 20 dB. Similarly to the width-modulated waveguides, an analysis of the refractive index profile indicates that the $TE_{20}$ mode is responsible for the QPM-DW generation (Fig. 4). Interestingly, peaks are observed corresponding to both odd- and even-order QPM, and effects up to the 16th QPM order are detectable. This situation differs from the preference for low, odd-ordered QPM effects in typical QPM materials (such as periodically poled lithium niobate, PPLN [26]), which usually employ a 50% duty-cycle modulation. In contrast, the cladding-modulated $Si_3N_4$ waveguides have short regions of oxide cladding, followed by long regions of fully air-clad $Si_3N_4$. This high-duty-cycle square wave is composed of both even- and odd-order harmonics, and, consequently, provides both even- and odd-order QPM. The simulated QPM-DW positions are in good agreement with the experiment for all grating orders and waveguide widths. Importantly, we see that QPM can still produce strong DWs with QPM orders of 8 or more, indicating that QPM for strongly phase-mismatched processes could be achieved with higher-order QPM instead of short modulation

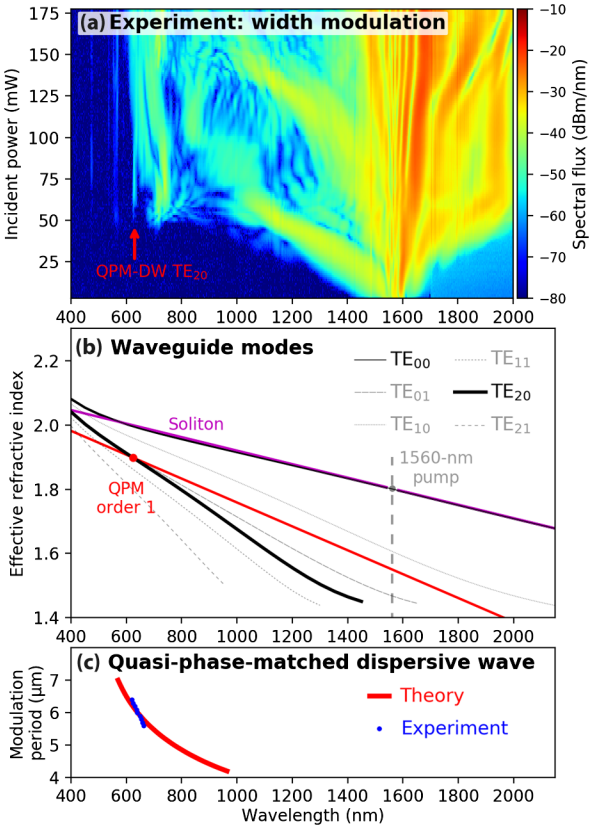


FIG. 2. (a) The spectrum of supercontinuum generation from a width-modulated waveguide as a function of input power. The arrow indicates the QPM DW to the $TE_{20}$ mode. (b) The effective refractive index of various modes of the waveguide as a function of wavelength. When the index of the soliton including a first order grating effect from the 6.2-μm width-modulation (red line) crosses the $TE_{20}$ mode, a QPM DW is generated. (c) The calculated spectral location of the $TE_{20}$ QPM DW as a function of the width-modulation period is in agreement with experimental results. The slight difference in slope may arise from irregularities in the dimensions of the waveguides.

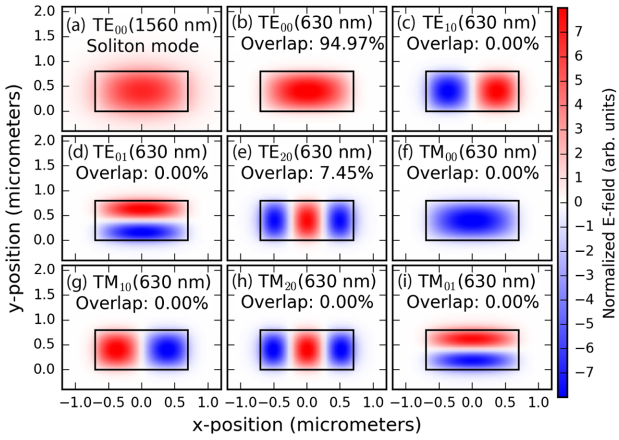


FIG. 3. Electric field profiles for the waveguide modes for a fully $SiO_2$-clad $Si_3N_4$ waveguide. (a) The $TE_{00}$ mode at 1560 nm, which is the expected mode of the soliton. (b)–(i) The electric field for various higher order modes at 630 nm, which is the approximate wavelength for the QPM-DW observed for the width-modulated waveguides. The result of the overlap integral of each mode with the $TE_{00}$ mode at 1560 nm is listed. Only the $TE_{00}$ and $TE_{20}$ modes have overlap integrals that are not vanishingly small. Note that for TM modes, $E_y$ is shown, while $E_x$ is shown for TE modes.

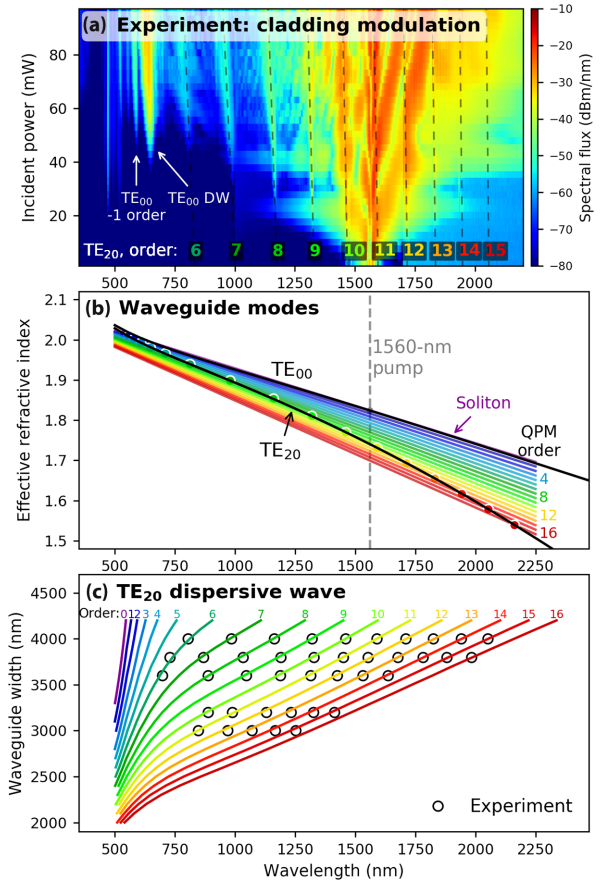


FIG. 4. (a) Supercontinuum generation from a 4000-nm-width cladding-modulated waveguide, showing many QPM-DW peaks resulting from QPM orders 6 to 15 to the $TE_{20}$ mode. The locations of the QPM DWs predicted by theory (dashed lines) agree with the experiment. QPM DWs to the $TE_{00}$ mode are indicated with arrows. (b) The effective index of the $TE_{00}$ and $TE_{20}$ modes, compared with the effective index of the soliton for various QPM orders (colorful lines). The dots indicate the location of the QPM DW in the $TE_{20}$ mode. (c) Calculations indicate that the locations of the QPM DWs change as a function of waveguide width, in agreement with experiment. Note that the sharp peaks in the 530-nm region of (a) are a result of third-harmonic generation to higher-order spatial modes [17].

periods, potentially avoiding fabrication difficulties and scattering loss. We also observe QPM-DW generation to the $TE_{00}$ mode [Fig. 4(a)], which is reproduced by numerical simulations using the nonlinear Schrödinger equation [42–44] (See Supplemental Material [32], Fig. S2).

This is the first demonstration of QPM to produce DWs in on-chip waveguides, but it is interesting to note that the QPM-DWs have been observed in a variety of situations. Indeed, the "Kelly sidebands" [45] seen in laser cavities and sidebands seen during soliton propagation in long-distance fiber links [46] are both examples of QPM DWs. QPM has also been demonstrated for both modulation instability as well as soliton-DW phase matching using width-oscillating fibers [27,29,31] and for fiber-Bragg gratings [47–51]. QPM has also been seen in Kerr frequency comb generation [52]. On-chip waveguides provide a powerful new platform for QPM-DW generation, offering straightforward dispersion engineering, access to a range of modulation periods, scalable fabrication, and the ability to access well-defined higher-order modes.

In this first demonstration, the spectral brightness of the QPM DWs was limited by several factors. First, most of the QPM DWs were generated in the $TE_{20}$ mode, which does not have optimal overlap with the $TE_{00}$ mode. Indeed, in the case where a $-1$-order QPM DW is generated in the $TE_{00}$ mode [Fig. 4(a)], the intensity of the light is higher. Second, for the cladding-modulated waveguides, we rely on a QPM structure with a high duty cycle, which effectively spreads the available QPM efficiency over many QPM orders, sacrificing efficiency in one particular order. Third, our waveguides only made modest changes to the effective mode area, and stronger QPM could be likely achieved with a deeper width modulation or stronger change in the cladding index. Finally, the QPM DWs are often produced far from the pump wavelength, in a spectral region where the soliton is dim. In future designs, optimized strategies for QPM-DW generation could utilize somewhat longer modulation periods, allowing QPM to the $TE_{00}$ mode, thereby maximizing mode overlap and allowing the QPM DWs to be located closer to the soliton central wavelength. Additionally, the waveguide modulation could be designed such that the efficiency of $\pm 1$ order QPM is optimized. All of these parameters can be modeled using software that calculates the modes of the waveguide. This fact, combined with the massive scalability of lithographic processing, should allow for rapid progress in designing optimized photonic waveguides for SCG.

Currently, designers of waveguide-SCG sources work in a limited parameter space: selecting materials and selecting the dimensions of the waveguide cross section. QPM opens a new dimension in the design space for photonic waveguides, one that is largely orthogonal to the other design dimensions. This orthogonality exists both in real space, since the QPM modulations exist in the light-propagation direction, but also in the waveguide-design space, as it provides a simple vertical shift of the phase-matching conditions with no bending of the index curve [Fig. 1(c)]. Consequently, it allows the spectral location of DWs to be modified with minimal effect on the GVD at the pump wavelength, which enables the soliton propagation conditions to be controlled separately from the DW phase-matching conditions. For example, using QPM, DWs could be produced even for purely anomalous GVD, greatly relaxing the requirements for material dispersion and waveguide cross section. Importantly, since the GVD at the pump is known to affect the noise properties of the SCG process [2], the ability to manipulate the locations of the DWs separately from the GVD could enable SCG sources that are simultaneously broadband and low noise. In addition, since similar

phase-matching conditions apply to SCG with picosecond pulses or continuous-wave lasers [2], QPM of the SCG process is likely not restricted to the regime of femtosecond pulses.

In summary, here we demonstrated that quasi-phase-matching is a powerful tool for controlling the supercontinuum generation process in on-chip photonic waveguides. We experimentally verified that a periodic modulation of either the waveguide width or cladding can allow $Si_3N_4$ waveguides to produce dispersive wave light at tunable spectral locations. By allowing dispersive waves to be quasi-phase-matched without significantly modifying the dispersion at the pump wavelength, this approach provides independent control over soliton compression and the spectral location of dispersive waves. Thus, quasi-phase-matching provides a new dimension in the design space for on-chip waveguides and allows supercontinuum sources to be tailored for the specific needs of each application.

We thank Jordan Stone, Nate Newbury, Michael Lombardi, and Chris Oates for providing helpful feedback on this manuscript. We thank Alexandre Kudlinski for his insightful comments on a draft of this Letter. This work is supported by AFOSR under Grant No. FA9550-16-1-0016, DARPA (DODOS and ACES programs), NIST, and NRC. This work is a contribution of the U.S. government and is not subject to copyright in the U.S.A.

*danhickstein@gmail.com

[1] R. R. Alfano, *The Supercontinuum Laser Source—The Ultimate White Light*, 3rd ed. (Springer, New York, 2016).
[2] J. M. Dudley, G. Genty, and S. Coen, Supercontinuum generation in photonic crystal fiber, Rev. Mod. Phys. **78**, 1135 (2006).
[3] G. P. Agrawal, *Nonlinear Fiber Optics* (Academic Press, New York, 2007).
[4] D. J. Jones, S. A. Diddams, J. K. Ranka, A. Stentz, R. S. Windeler, J. L. Hall, and S. T. Cundiff, Carrier-envelope phase control of femtosecond mode-locked lasers and direct optical frequency synthesis, Science **288**, 635 (2000).
[5] R. Holzwarth, Th. Udem, T. W. Hansch, J. C. Knight, W. J. Wadsworth, and P. St. J. Russell, Optical Frequency Synthesizer for Precision Spectroscopy, Phys. Rev. Lett. **85**, 2264 (2000).
[6] S. A. Diddams, D. J. Jones, J. Ye, S. T. Cundiff, J. L. Hall, J. K. Ranka, R. S. Windeler, R. Holzwarth, T. Udem, and T. W. Hansch, Direct Link between Microwave and Optical Frequencies with a 300 THz Femtosecond Laser Comb, Phys. Rev. Lett. **84**, 5102 (2000).
[7] T. Betz, J. Teipel, D. Koch, W. Hartig, J. R. Guck, J. Käs, and H. W. Giessen, Excitation beyond the monochromatic laser limit: simultaneous 3-D confocal and multiphoton microscopy with a tapered fiber as white-light laser source, J. Biomed. Opt. **10**, 054009 (2005).
[8] I. Coddington, N. Newbury, and W. Swann, Dual-comb spectroscopy, Optica **3**, 414 (2016).
[9] S. Moon and D. Y. Kim, Ultra-high-speed optical coherence tomography with a stretched pulse supercontinuum source, Opt. Express **14**, 11575 (2006).
[10] A. Klenner, A. S. Mayer, A. R. Johnson, K. Luke, M. R. E. Lamont, Y. Okawachi, M. Lipson, A. L. Gaeta, and U. Keller, Gigahertz frequency comb offset stabilization based on supercontinuum generation in silicon nitride waveguides, Opt. Express **24**, 11043 (2016).
[11] M. A. G. Porcel, F. Schepers, J. P. Epping, T. Hellwig, M. Hoekman, R. G. Heideman, P. J. M. van der Slot, C. J. Lee, R. Schmidt, R. Bratschitsch, C. Fallnich, and K.-J. Boller, Two-octave spanning supercontinuum generation in stoichiometric silicon nitride waveguides pumped at telecom wavelengths, Opt. Express **25**, 1542 (2017).
[12] A. S. Mayer, A. Klenner, A. R. Johnson, K. Luke, M. R. E. Lamont, Y. Okawachi, M. Lipson, A. L. Gaeta, and U. Keller, Frequency comb offset detection using supercontinuum generation in silicon nitride waveguides, Opt. Express **23**, 15440 (2015).
[13] J. P. Epping, T. Hellwig, M. Hoekman, R. Mateman, A. Leinse, R. G. Heideman, A. van Rees, P. J. M. van der Slot, C. J. Lee, C. Fallnich, and K.-J. Boller, On chip visible-to-infrared supercontinuum generation with more than 495 THz spectral bandwidth, Opt. Express **23**, 19596 (2015).
[14] B. Kuyken, T. Ideguchi, S. Holzner, M. Yan, T. W. Hänsch, J. Van Campenhout, P. Verheyen, S. Coen, F. Leo, R. Baets, G. Roelkens, and N. Picqué, An octave-spanning mid-infrared frequency comb generated in a silicon nanophotonic wire waveguide, Nat. Commun. **6**, 6310 (2015).
[15] J. M. Chavez Boggio, D. Bodenmüller, T. Fremberg, R. Haynes, M. M. Roth, R. Eisermann, M. Lisker, L. Zimmermann, and M. Böhm, Dispersion engineered silicon nitride waveguides by geometrical and refractive-index optimization, J. Opt. Soc. Am. B **31**, 2846 (2014).
[16] D. Carlson, D. Hickstein, A. Lind, J. Olson, R. Fox, R. Brown, A. Ludlow, Q. Li, D. Westly, H. Leopardi, T. Fortier, K. Srinivasan, S. Diddams, and S. Papp, Photonic-Chip Supercontinuum with Tailored Spectra for Counting Optical Frequencies, Phys. Rev. Applied **8**, 014027 (2017).
[17] D. R. Carlson, D. D. Hickstein, A. Lind, S. Droste, D. Westly, N. Nader, I. Coddington, N. R. Newbury, K. Srinivasan, S. A. Diddams, and S. B. Papp, Self-referenced frequency combs using high-efficiency silicon-nitride waveguides, Opt. Lett. **42**, 2314 (2017).
[18] D. Y. Oh, K. Y. Yang, C. Fredrick, G. Ycas, S. A. Diddams, and K. J. Vahala, Coherent ultra-violet to near-infrared generation in silica ridge waveguides, Nat. Commun. **8**, 13922 (2017).
[19] D. D. Hickstein, H. Jung, D. R. Carlson, A. Lind, I. Coddington, K. Srinivasan, G. G. Ycas, D. C. Cole, A. Kowligy, C. Fredrick, S. Droste, E. S. Lamb, N. R. Newbury, H. X. Tang, S. A. Diddams, and S. B. Papp, Ultrabroadband Supercontinuum Generation and Frequency-Comb Stabilization Using On-Chip Waveguides with Both Cubic and Quadratic Nonlinearities, Phys. Rev. Applied **8**, 014025 (2017).
[20] R. Driben, A. V. Yulin, and A. Efimov, Resonant radiation from oscillating higher order solitons, Opt. Express **23**, 19112 (2015).

[21] J. McLenaghan and F. König, Few-cycle fiber pulse compression and evolution of negative resonant radiation, New J. Phys. **16**, 063017 (2014).
[22] N. Akhmediev and M. Karlsson, Cherenkov radiation emitted by solitons in optical fibers, Phys. Rev. A **51**, 2602 (1995).
[23] R. W. Boyd, *Nonlinear Optics*, 3rd ed. (Academic Press, Amsterdam, Boston, 2008).
[24] P. A. Franken and J. F. Ward, Optical harmonics and nonlinear phenomena, Rev. Mod. Phys. **35**, 23 (1963).
[25] J. A. Armstrong, N. Bloembergen, J. Ducuing, and P. S. Pershan, Interactions between light waves in a nonlinear dielectric, Phys. Rev. **127**, 1918 (1962).
[26] M. M. Fejer, G. A. Magel, D. H. Jundt, and R. L. Byer, Quasi-phase-matched second harmonic generation: Tuning and tolerances, IEEE J. Quantum Electron. **28**, 2631 (1992).
[27] A. Kudlinski, A. Mussot, M. Conforti, and S. Trillo, Parametric excitation of multiple resonant radiations from localized wave packets, Sci. Rep. **5**, 9433 (2015).
[28] K. Luo, Y. Xu, M. Erkintalo, and S. G. Murdoch, Resonant radiation in synchronously pumped passive Kerr cavities, Opt. Lett. **40**, 427 (2015).
[29] M. Conforti, S. Trillo, A. Kudlinski, and A. Mussot, Multiple QPM resonant radiations induced by MI in dispersion oscillating fibers, IEEE Photonics Technol. Lett. **28**, 740 (2016).
[30] L. G. Wright, S. Wabnitz, D. N. Christodoulides, and F. W. Wise, Ultrabroadband Dispersive Radiation by Spatiotemporal Oscillation of Multimode Waves, Phys. Rev. Lett. **115**, 223902 (2015).
[31] M. Droques, A. Kudlinski, G. Bouwmans, G. Martinelli, and A. Mussot, Dynamics of the modulation instability spectrum in optical fibers with oscillating dispersion, Phys. Rev. A **87**, 013813 (2013).
[32] See Supplemental Material at http://link.aps.org/supplemental/10.1103/PhysRevLett.120.053903 for additional information regarding the experiment and simulations of pulse propagation.
[33] M. H. P. Pfeiffer, A. Kordts, V. Brasch, M. Zervas, M. Geiselmann, J. D. Jost, and T. J. Kippenberg, Photonic Damascene process for integrated high-Q microresonator based nonlinear photonics, Optica **3**, 20 (2016).
[34] L. C. Sinclair, J.-D. Deschénes, L. Sonderhouse, W. C. Swann, I. H. Khader, E. Baumann, N. R. Newbury, and I. Coddington, A compact optically coherent fiber frequency comb, Rev. Sci. Instrum. **86**, 081301 (2015).
[35] D. D. Hickstein, G. C. Kerber, C. Fredrick, and D. R. Carlson, GracefulOSA, https://github.com/DanHickstein/gracefulOSA (2017).
[36] A. B. Fallahkhair, K. S. Li, and T. E. Murphy, Vector finite difference mode solver for anisotropic dielectric waveguides, J. Lightwave Technol. **26**, 1423 (2008).
[37] L. Bolla, EMPy—Electromagnetic Python, https://github.com/lbolla/EMpy (2017).
[38] K. Luke, Y. Okawachi, M. R. E. Lamont, A. L. Gaeta, and M. Lipson, Broadband mid-infrared frequency comb generation in a $Si_3N_4$ microresonator, Opt. Lett. **40**, 4823 (2015).
[39] I. H. Malitson, Interspecimen Comparison of the refractive index of fused silica, J. Opt. Soc. Am. **55**, 1205 (1965).
[40] Q. Lin, O. J. Painter, and G. P. Agrawal, Nonlinear optical phenomena in silicon waveguides: Modeling and applications, Opt. Express **15**, 16604 (2007).
[41] X. Guo, C.-L. Zou, and H. X. Tang, Second-harmonic generation in aluminum nitride microrings with 2500%/W conversion efficiency, Optica **3**, 1126 (2016).
[42] A. M. Heidt, Efficient adaptive step size method for the simulation of supercontinuum generation in optical fibers, J. Lightwave Technol. **27**, 3984 (2009).
[43] J. Hult, A Fourth-Order Runge-Kutta in the Interaction Picture Method for Simulating Supercontinuum Generation in Optical Fibers, J. Lightwave Technol. **25**, 3770 (2007).
[44] G. Ycas, D. Maser, and D. D. Hickstein, pyNLO—Nonlinear optics modeling for Python (2016).
[45] S. M. J. Kelly, Characteristic sideband instability of periodically amplified average soliton, Electron. Lett. **28**, 806 (1992).
[46] F. Matera, A. Mecozzi, M. Romagnoli, and M. Settembre, Sideband instability induced by periodic power variation in long-distance fiber links, Opt. Lett. **18**, 1499 (1993).
[47] P. S. Westbrook, J. W. Nicholson, K. S. Feder, Y. Li, and T. Brown, Supercontinuum generation in a fiber grating, Appl. Phys. Lett. **85**, 4600 (2004).
[48] K. Kim, S. A. Diddams, P. S. Westbrook, J. W. Nicholson, and K. S. Feder, Improved stabilization of a 1.3 μm femtosecond optical frequency comb by use of a spectrally tailored continuum from a nonlinear fiber grating, Opt. Lett. **31**, 277 (2006).
[49] L. M. Zhao, C. Lu, H. Y. Tam, D. Y. Tang, L. Xia, and P. Shum, Observation of spectral enhancement in a soliton fiber laser with fiber Bragg grating, Opt. Express **17**, 3508 (2009).
[50] D.-I. Yeom, J. A. Bolger, G. D. Marshall, D. R. Austin, B. T. Kuhlmey, M. J. Withford, C. Martijn de Sterke, and B. J. Eggleton, Tunable spectral enhancement of fiber supercontinuum, Opt. Lett. **32**, 1644 (2007).
[51] P. S. Westbrook and J. W. Nicholson, Perturbative approach to continuum generation in a fiber Bragg grating, Opt. Express **14**, 7610 (2006).
[52] S.-W. Huang, A. K. Vinod, J. Yang, M. Yu, D.-L. Kwong, and C. W. Wong, Quasi-phase-matched multispectral Kerr frequency comb, Opt. Lett. **42**, 2110 (2017).